Electronic Supplementary Information (ESI) for

Multicolor Carbon Dots Doped Nanofibrous Membrane for Unclonable Anti-Counterfeiting and Data Encryption

Shunfei Qiang,[1,§] Ke Yuan,[2,§] Yanyan Cheng,[1] Guoqiang Long,[3] Wenkai Zhang,[1,*] Xiaofeng Lin,[4] Xiuli Chai,[3,*] Xiaomin Fang[1] and Tao Ding[1]

[1]Henan Engineering Research Center of Functional Materials and Catalytic Reactions, College of Chemistry and Chemical Engineering, Henan University, Kaifeng 475004, China.

[2]School of Computer and Information Engineering, Henan University, Kaifeng, 475004, China.

[3]School of Artificial Intelligence, Henan University, Zhengzhou 450046, China.

[4]School of Chemical Engineering and Light Industry, Guangdong University of Technology, Guangzhou 510006, China.

*E-mail: zhangwenkai@henu.edu.cn (W.Z.); chaixiuli@henu.edu.cn (X.C.)

Tel: +86 (0371) 2388-1589

Contents

S1. FT-IR Spectra

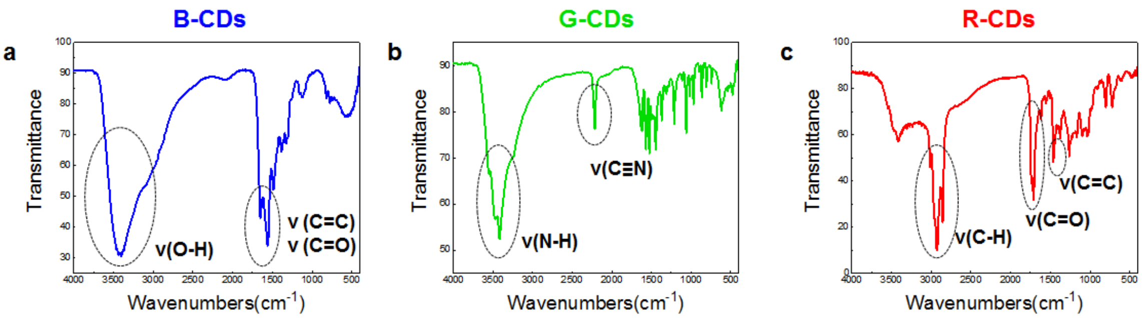

Fig. S1 FT-IR spectra of B-, G-, and R-CDs. (a) B-CDs have a strong and wide absorption peak of the O-H bond in the COOH (3700-2500 cm^{-1}), and show significant C=C bonds in the aromatic ring skeleton at 1560 cm^{-1}, stretching vibration of C=O bond at 1653 cm^{-1}; (b) G-CDs have stretching vibrations of N-H (3475 cm^{-1} and 3415 cm^{-1}) and C≡N (2210 cm^{-1}) bonds; (c) R-CDs show stretching vibration of C=O (≈1710 cm^{-1}) and C=C (1460 cm^{-1}) bonds. Additionally, the C-H bond in alkanes has a sharp absorption peak at 2928 cm^{-1}.

S2. Crosslinking of Nanofibers

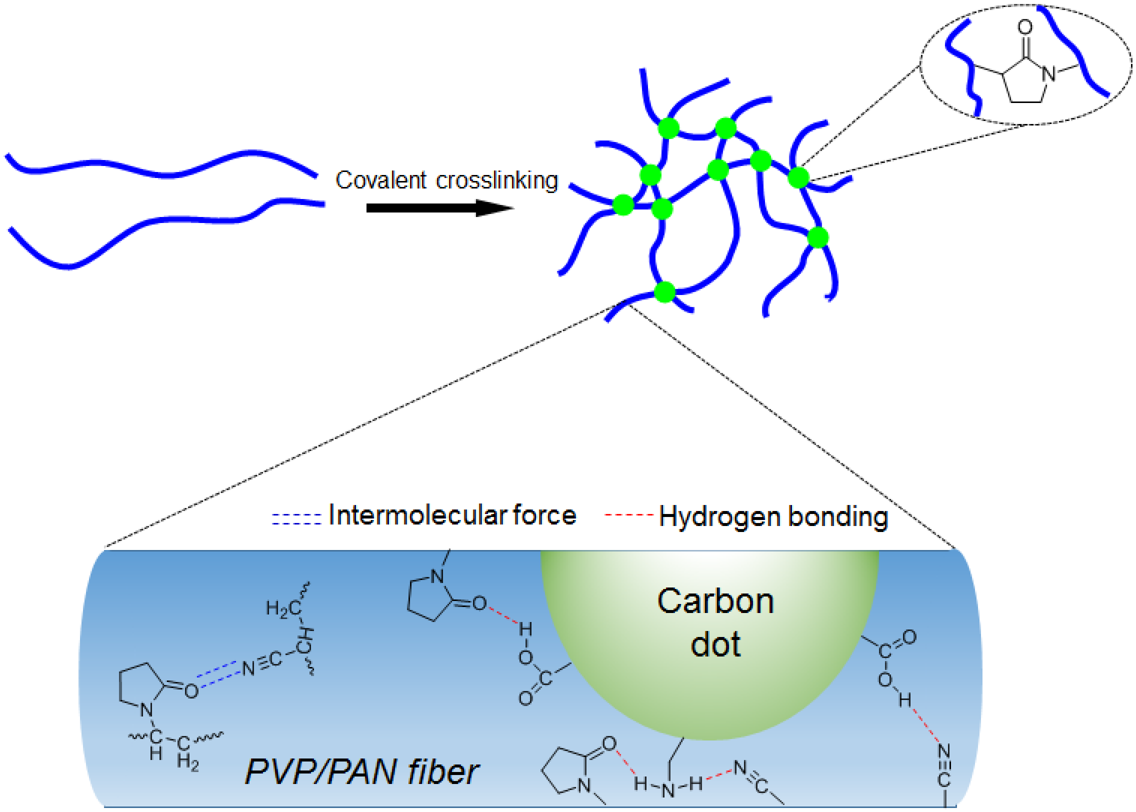

Fig. S2 The diagram of nanofiber crosslinking. Crosslinking of PVP with persulfate involves abstraction of a hydrogen atom from the polymer chain by an SO_4^{2-} or OH radicals. The macromolecular radicals thus formed moves by virtue of molecular or segmental diffusion to another macromolecule radical and forms a stable covalent crosslinking. In addition, carboxyl and amine groups on the carbon dots produce a large amount of hydrogen bonding with pyrrolidone groups on the PVP matrix.

S3. Effect of Substrate on Fiber Patterns

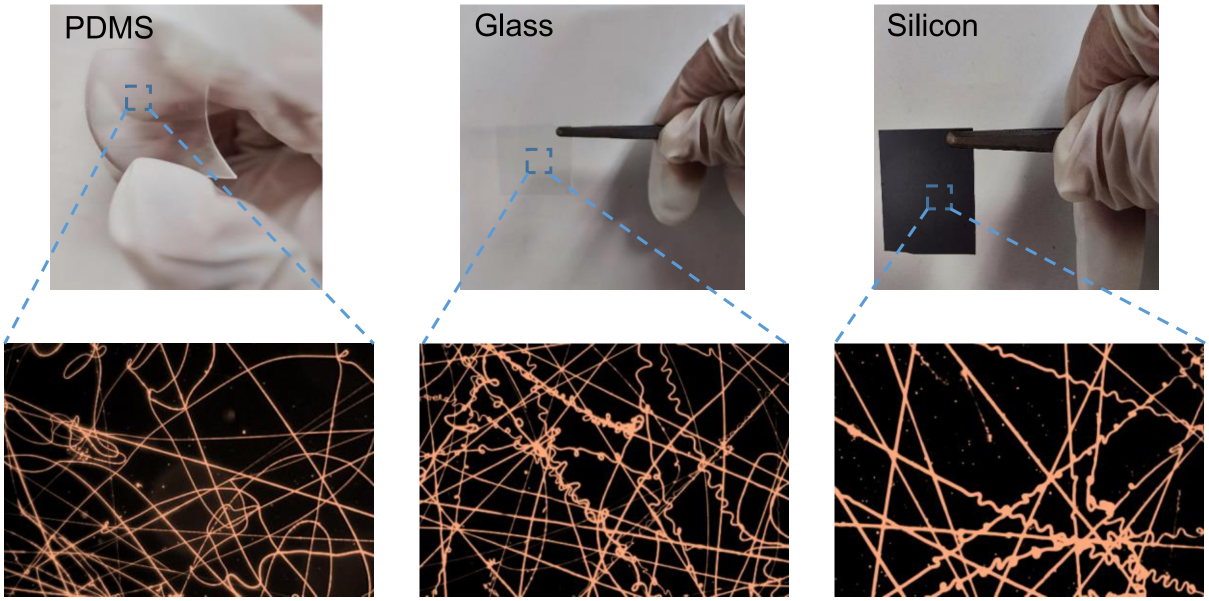

Fig. S3 Photographs of PUF tags fabricated with different substrates: from left to right, PDMS, glass, silicon. The optical images of ESNFs on corresponding substrates are placed below. Electrospinning conditions: polymer solution, 10wt% DMF solution of PU; applied voltage U = 10 kV; spinneret-to-collector distance d = 20 cm; injection speed V_J = 5 μL/min; electrospinning time t = 180 s. The ambient temperature was 27.2 °C and the relative humidity was 44%.

S4. Effect of Polymer on Fiber Patterns

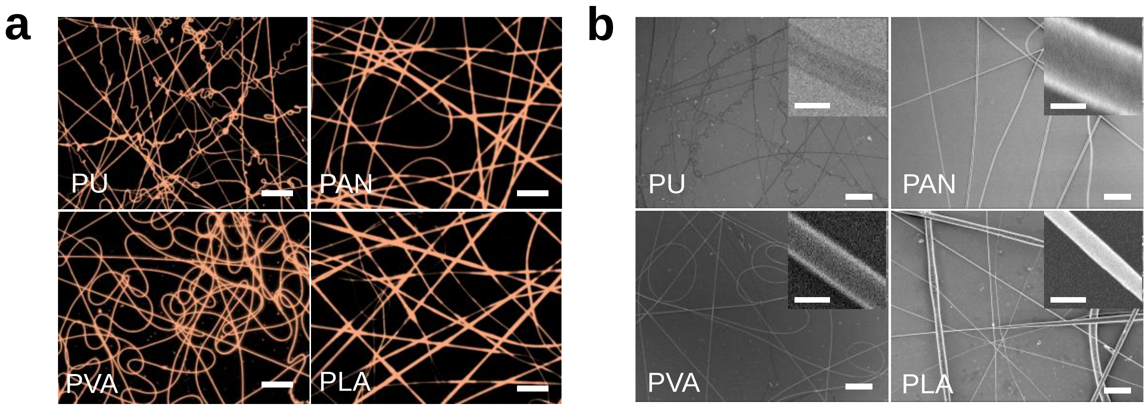

Fig. S4 (a) Dark-field scattering and (b) SEM images of the electrospun PU, PAN, PVA and PLA fibers. Polymer solution, 10 wt% DMF solution of PU; 10 wt% DMF solution of PAN; 10wt % aqueous solution of PVA; 10wt % chloroform solution of PLA. Electrospinning parameters: applied voltage U = 10 kV; spinneret-to-collector distance d = 20 cm; injection speed V_J = 5 μL/min; electrospinning time t = 180 s; substrate, glass. The ambient temperature was 27.2 °C and the relative humidity was 44%. The scale bars for images of (a), (b) and the insets of (b) are 2 μm, 10 μm, and 500 nm, respectively.

S5. White Light Emission

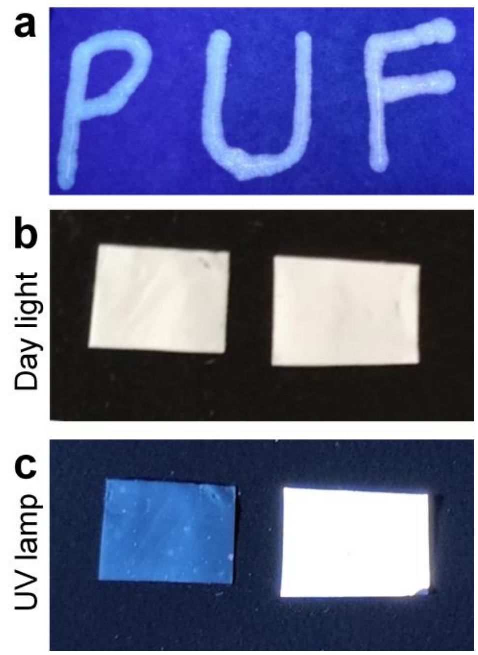

Fig. S5 (a) Photograph of “PUF” patterned with mixed RGB fluorescent CD ink on the ESNF membrane. (b, c) Photograph of CD-free (left) and CD-doped (right) electrospun membrane under day light (b) and 365 nm UV lamp (c).

S6. Morphologies of Nanofiber Membranes

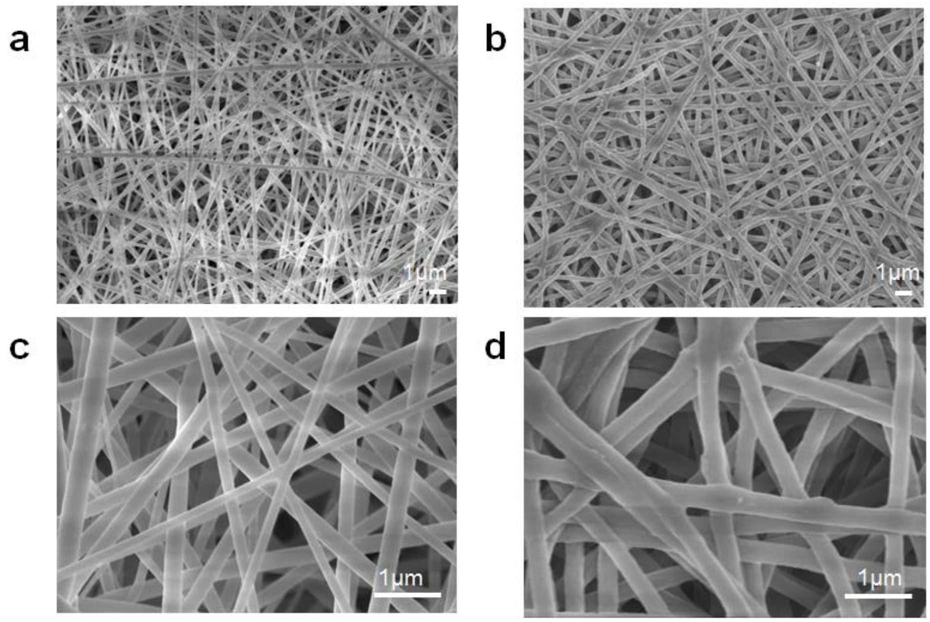

Fig. S6 SEM images of PVP/PAN fiber membranes. (a) non-crosslinked; (b) crosslinked. (c) and (d) are magnified images for (a) and (b), respectively.

S7. Mechanical Strength

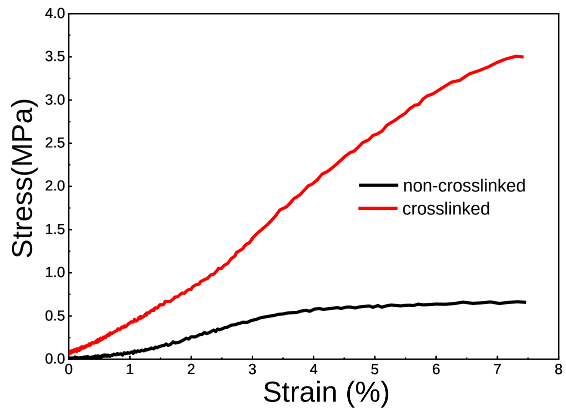

Fig. S7 The comparisons of the mechanical properties of PVP/PAN fibrous membranes before and after cross-linking. For the non-crosslinked fibrous membrane, the tensile strength is 0.65 MPa at the tensile fracture strain. After crosslinking, the tensile strength of the electrospun PVP/PAN membrane increases to 3.5 MPa, while the tensile fracture strains before and after crosslinking are similar, with values of 7.48% and 7.43% respectively.

S8. Thermal Stability of Membrane

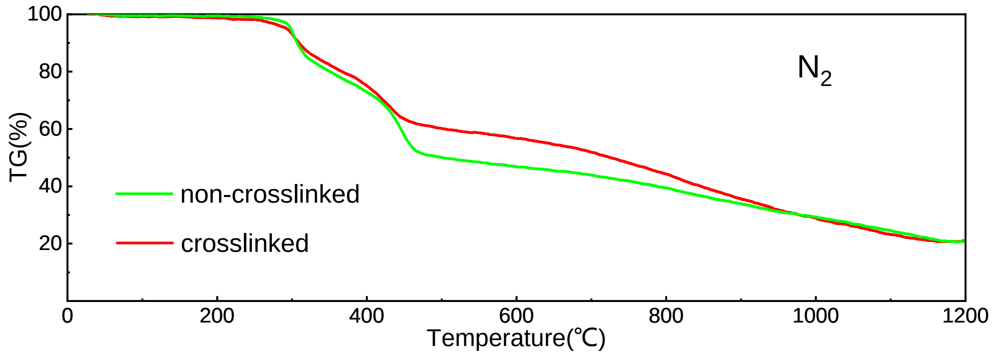

Fig. S8 Thermogravimetric analysis curves of PVP/PAN fibers before and after crosslinking. Instrument: Mettler Toledo TGA/SDTA851e thermogravimetric analyzer; heating rate: 10°C·min^{-1}; atmosphere: nitrogen.

S9. Fluorescence Filters

Table S1 Excitation (EX)/emission (EM) wavelengths of fluorescence filters of the fluorescence microscope and RGB-CDs.

Filters/Dyes	EX (nm)	EM (nm)
DAPI	365	445±25
eGFP	470±20	525±25
CY3	545±25	605±35
B-CDs	360	428
G-CDs	430	510
R-CDs	550	610

S10. PLQY Measurements

Table S2 The PLQY measurements of B-, G-, and R-CDs

Quinine sulfate				**B-CDs**			
$\lambda_{ex/nm}$	A_1*	F_1*	QY_1*	$\lambda_{ex/nm}$	A_1	F_1	QY_1
360	0.0302	23802	0.69	360	0.0295	19193	0.57
Coumarin-6				**G-CDs**			
$\lambda_{ex/nm}$	A_2*	F_2*	QY_2*	$\lambda_{ex/nm}$	A_2	F_2	QY_2
430	0.0482	26169	0.8	430	0.042	8329	0.29
Rhodamine B				**R-CDs**			
$\lambda_{ex/nm}$	A_3*	F_3*	QY_3*	$\lambda_{ex/nm}$	A_3	F_3	QY_3
550	0.063	3467	0.89	550	0.0702	497	0.11

$\lambda_{ex/nm}$, excitation wavelength; *A**, absorbance of reference fluorophore; *F**, integral fluorescence intensity of reference fluorophore; *QY**, quantum efficiency of reference fluorophore; *A*, absorbance of carbon dots; *F*, integral fluorescence intensity of carbon dots; *QY*, quantum efficiency of carbon dots.

S11. Stability of CD Inks

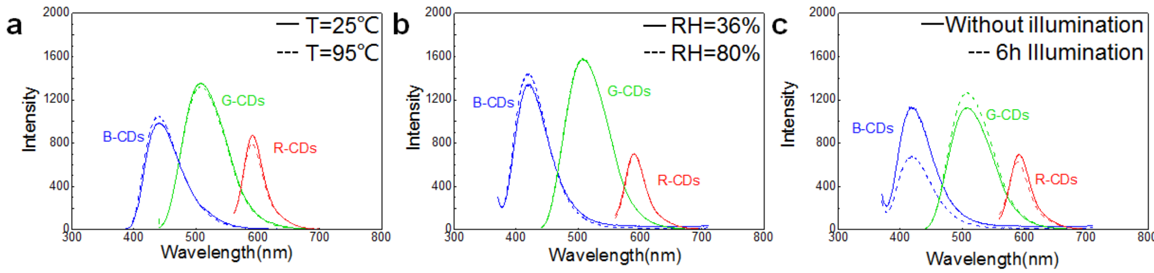

Fig. S9 (a) Thermo, (b) moisture and (c) photostability investigation of B-, G- and R-CD inks by monitoring the fluorescence spectra. (a) Solid, room temperature; dash, heating at 95 °C for 1 h. (b) Solid, ambient conditions with 36% RH; dash, exposing to 80% RH air (produced by saturated KBr solution). (c) Solid, ambient conditions without irradiation; dash, illumination by Xe lamp (PLS-SXE 300W, 65 mW/cm^2) for 6 h.

S12. Details of Perceptional Hashing

Perceptual image hashing is a family of algorithms that generate content-based image hashes. Unlike cryptographic hashes, perceptual hashes are designed to not change much when an image undergoes minor modifications such as compression, colorcorrection, and brightness.

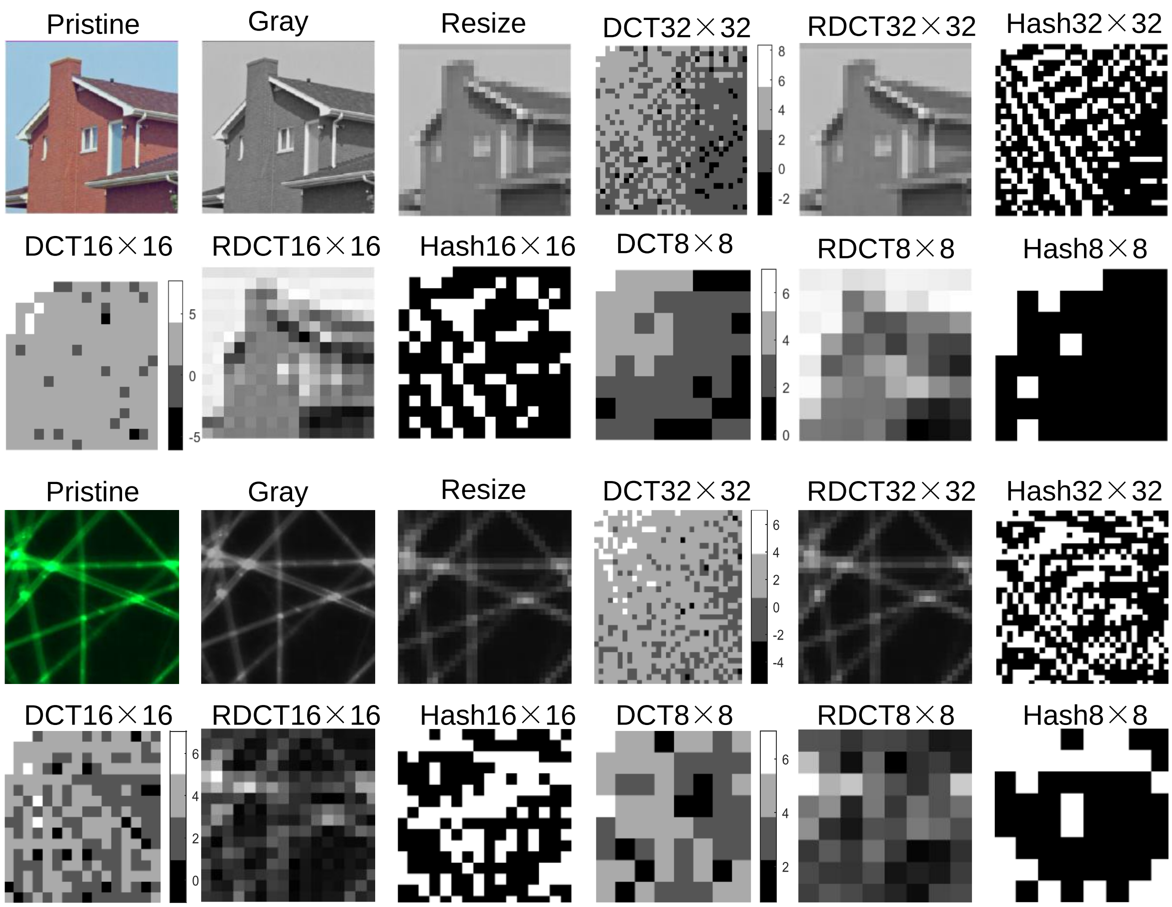

Fig. S10 Different stages of perceptional hashing for 'House' (1st and 2nd columns) and electrospun fiber (3rd and 4th columns) images. From left to right: pristine image, Gray-scaled image, resized image, DCT coefficients, reverse-DCT (RDCT), hash values.

Perceptual hashing algorithms use perceptual features of images to generate their hashes. The primary goal is to generate hashes that remain unchanged or change slightly when content preserving modifications are made to the image. The main three steps involved in perceptual hashing algorithms are image pre-processing, perceptual feature extraction, and quantization or compression to generate the final hash string. There are various perceptual hashing algorithms that vary from each other in the way they extract perceptual features from the image. Take the images ‘House’ and electrospun fibers as comparative examples (**Fig. S10**):

1. Pre-processing

In the pre-processing phase, an input image is prepared for feature extraction. This step reduces the size of the data that needs to be processed at a later stage, reducing the overall processing time. The pre-processing steps include graying and resizing. Images might be resized to evaluate all inputs at a common size (32×32 pixels).

2. Feature extraction

In perceptual hashing, the features extracted from an image should be invariant to content preserving manipulation. There are mainly two types of techniques used for general feature extraction, (a) frequency domain transformation such as Discrete Fourier Transform (DFT), Discrete Cosine Transform (DCT), Discrete Wavelet Transform (DWT), Fourier-Mellin transform and (b) dimensionality reduction techniques such as Principal Component Analysis (PCA), Non-Negative Matrix Factorization (NMF) and Singular Value Decomposition (SVD). Here, we use the Discrete Cosine Transform (DCT) to extract the random fiber features. The DCT of an image is computed by projecting the image onto a fixed coefficient matrix in the frequency domain by expressing each pixel as the sum of cosine components of their Fourier Transform. As the DCT has a strong "energy compactness" property, most of the image information concentrates on low frequency DCT coefficients. These low frequency components are mostly stable under any content preserving manipulation but sensitive to changes in perceptual features such as adding or removing objects. In our cases, DCT of the 32×32 image is computed which results in 32×32 coefficients matrix where each coefficient is denoted by C_{ij}, (i = 0…31, j = 0…31). Then the top left 32×32, 16×16 and 8×8 lower frequency coefficients are respectively selected for the final hash calculation. *RDCT* images in **Fig. S10** show how they look like after the DCT extraction steps.

3. Quantization and hash generation

Numerical values that represent features of an image can be quantized, generating a fixed sized hash which is a compact and somewhat unique representation of an image. Statistical properties of features are often used for quantization. In DCT algorithms, the DCT coefficients are quantized by comparing each coefficient with the median or mean of the coefficients. After DCT extraction, each coefficient is quantized by comparing with the median (C_m) of all coefficients, where C_{ij} = 0 if $C_{ij} \leq C_m$ and 1 otherwise. The final hashes are 64, 256 and 1024-bit string, respectively.

S13. Fingerprint Length Dependence

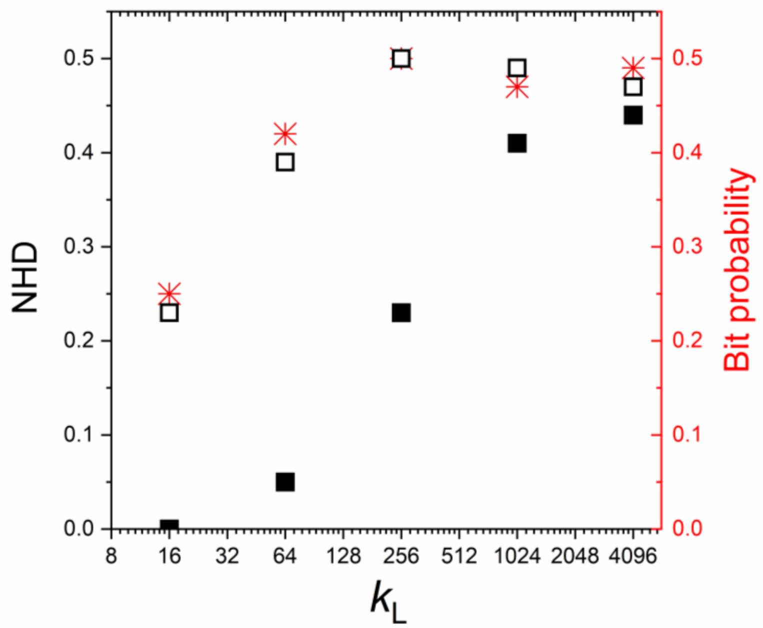

Fig. S11 The calculated intra and inter NHDs and bit probabilities when the features are encoded as different fingerprint lengths (k_L, i.e., the output hash lengths from phash extraction). Inter NHD, black hollow square; intra NHD, black solid square; bit probability, red star. When the k_L is 256 bits, inter and intra NHD have large gap and simultaneously uniform 0,1-bit probability.

S14. False Positive Rate and False Negative Rate

The False Positive Rate (FPR) and False Negative Rate (FRR) can be calculated by the following formulas:

$$FPR = \sum_{i}^{P} \sum_{j}^{Q} \frac{FPR_{i,j}}{PQ}, \tag{1}$$

$$FPR_{i,j} = \sum_{i' \neq i}^{P} \sum_{m}^{K} \sum_{n}^{K} \frac{Com(T, D(r_{m,i,j}, r_{n,i'.j}))}{K^2(P-1)} \tag{2}$$

$$FNR = \sum_{i}^{P} \sum_{j}^{Q} \frac{FNR_{i,j}}{PQ} \tag{3}$$

$$FNR_{i,j} = \sum_{m}^{K} \sum_{n}^{K} \frac{Com(D(r_{m,i,j}, r_{n,i.j}), T)}{K^2} \tag{4}$$

$$Com\left(T, D(r_{m,i,j}, r_{n,i'.j})\right) = \begin{Bmatrix} 1, T < D(r_{m,i,j}, r_{n,i'.j}) \\ 0, T \geq D(r_{m,i,j}, r_{n,i'.j}) \end{Bmatrix} \tag{5}$$

where *P* is the number of devices to be evaluated, *K* is the number of tests on each device for each challenge, $D(r_{m,i,j}, r_{n,i'.j})$ refers to the inter or intra distance between the *m*th response of the *j*th challenge of the *i*th device and the *n*th response of the *j*th challenge of the *i'*th device. The authentication threshold *T* is set according to the practical security requirements.

S15. Stability of ESNF-PUF Patterns

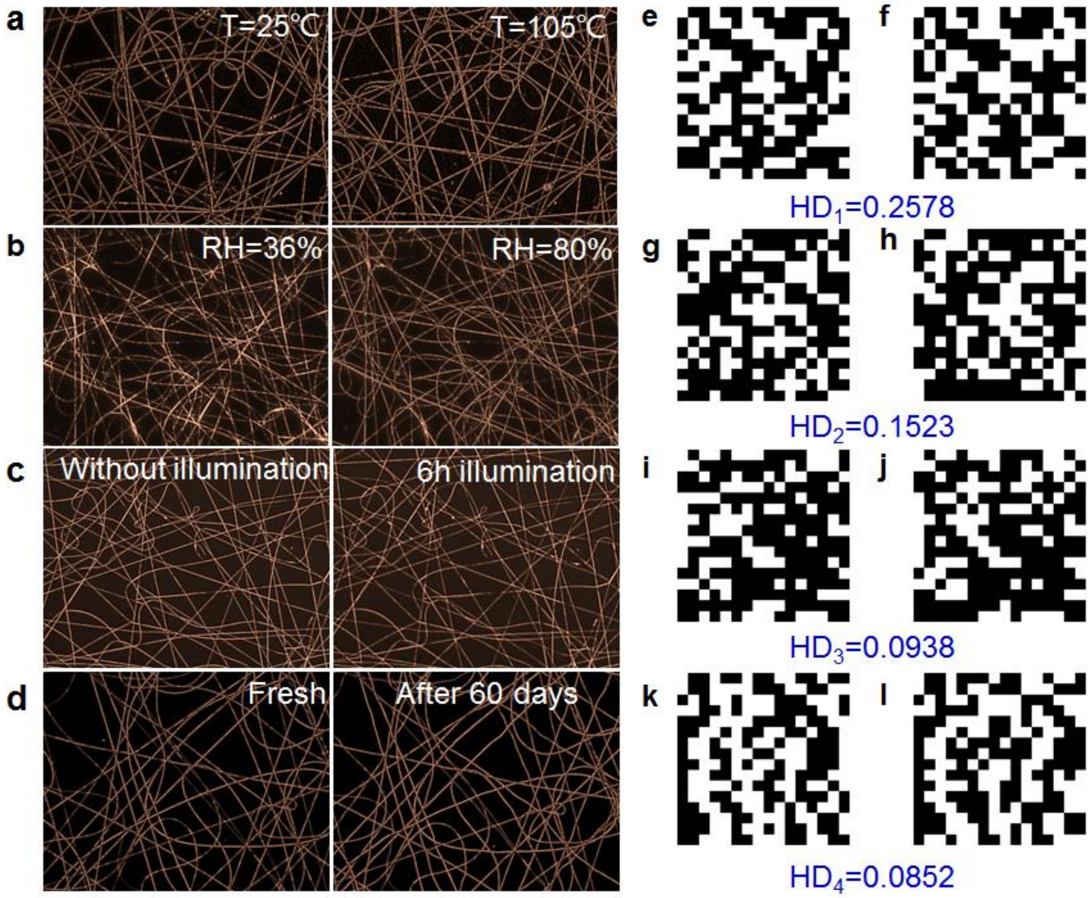

Fig. S12 (a) Thermo, (b) moisture, (c) photostability and (d) long-term duration of ESNF-PUFs by monitoring the dark field scattering images. (a) Left, room temperature; right, heating at 105 °C for 1 h. (b) Left, ambient conditions with 36% RH; right, exposing to 80% RH air (produced by saturated KBr solution). (c) Left, ambient conditions without irradiation; right, illumination by Xe lamp (PLS-SXE 300W, 65 mW/cm^2) for 6 h. (c) Left, ambient conditions without irradiation; right, illumination by Xe lamp (PLS-SXE 300W, 65 mW/cm^2) for 6 h. (d) Left, fresh sample; right, capturing the same sensor after 60 days. The tags were stored at 22 ± 2 °C and 40–50% relative humidity in the dark. (e-h) The corresponding hash values for (a-d), respectively. The Hamming distances of two images are shown below.

S16. Robustness Under Non-Ideal Handling Conditions

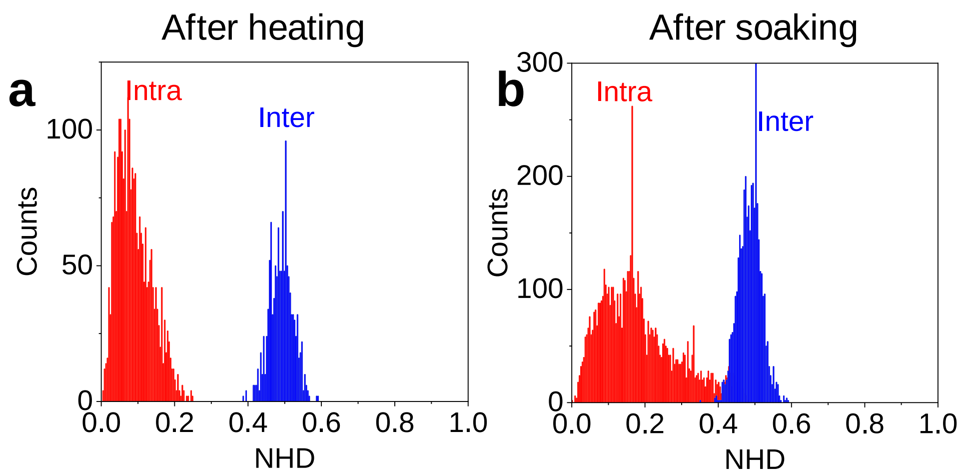

Fig. S13 Distributions of normalized Hamming distances (NHD) after subjecting ESNF-PUF to non-ideal treatments: 120 °C heating for 2h (a) and soaking in water (b). The distributions remain well separated even under these adverse conditions.

S17. Overview of Optical PUFs

Table S3 Selected reports of optical PUFs.

Optical PUF	**Entropy source**	**CRP**[a]	**Algorithm**	k_L[b] **(bits)**	S **(bit)**	**Robustness**	**Storage density (bit/cm²)**	**Internal/ External**	**Ref**
polymer composite	laser speckle	Laser-coherent scattering	Gabor hash	2400	233	FRR[c]~10^{-2}	5.7×10^{13}	External	1
paper	surface roughness	Laser-speckle	Binary hash	1600-4000	72	n.a. [d]	8.2×10^{4}	Internal	2
paper	surface roughness	WL[e]-reflectivity	Feature vector	3200	n.a.	FPR[f]~10^{-96}	5.5×10^{1}	Internal	3
paper	rexture speckle	LED-Scattering	Gabor hash	~200,000	43	FPR~5%	7.9×10^{5}	Internal	4
paper	fibers	UV-Fluorescence	Gray code	96	72	FPR<10%	2.6×10^{2}	Internal	5
silicon photonics	chaotic optical near field	laser-transmission	wavelet analysis	8000	n.a	n.a.	3.2×10^{6}	Internal	6
silicon photonics	chaotic optical near field	pulsed laser-transmission	Binary hash	128	256	n.a.	3.6×10^{8}	Internal	7
ESNF	electrostatic bending	WL-scattering	Hough-Gray code	512	260	SC[g]>80%	5.1×10^{2}	Internal	8

Natural silk	pinhole	LED-diffraction	Binary hash	768	345	BER[h]<10^{-4}	6.4×10^{3}	External	9
Plasmonic antenna	Brownian diffusion	UV-Fluorescence	n.a.	n.a.	n.a.	n.a.	n.a.	External	10
Photonic crystal	colloidal assembly	WL-reflectivity	Binary hash	2500	n.a.	0.99	2.5×10^{5}	External	11
Photonic crystal	colloidal assembly	WL-reflectivity	Machine learning	n.a.	n.a.	n.a.	n.a.	External	12
Chaotic metasurface	Ion beam etching	UV-Fluorescence	Gabor hash	1.12M	156250	FAR/FRR[i]~10^{-300}	2.6×10^{13}	External	13
plasmonic nanoparticles	Brownian diffusion	WL-plasmon scattering	Machine learning	n.a.	n.a.	n.a.	n.a.	External	14
Microdiamond	spin-coating	Laser-Raman	Binary hash	10000	n.a.	n.a.	1.6×10^{7}	External	15
Polymer dewetting	Dewetting	Laser-Raman	Binary hash	256	n.a.	n.a.	1.0×10^{7}	External	16
Organic semiconductors	drop-casting	UV-Fluorescence	Binary hash	256	n.a.	n.a.	1.0×10^{7}	Internal	17
laser dye	Random laser	wavelength-laser	Binary hash	n.a.	n.a.	n.a.	n.a	Internal	18

Wrinkle	Laser abalation	WL-reflectivity	Machine learning	n.a.	n.a.	n.a.	n.a.	Internal	19
Fluorescence protein	drop-casting	UV-Fluorescence	Binary hash	256	120	FAR/FRR ~10^{-12}	1.0×10^{5}	External	20
Plasmonic antenna	drop-casting	Laser-Raman	Binary hash	2500	n.a.	n.a.	1.0×10^{6}	External	21
plasmonic nanopapers	self-assembly	Laser-Raman	n.a.	n.a.	n.a.	n.a.	n.a.	Internal	22
ink droplets	Dewetting	UV-Fluorescence	Machine learning	n.a.	n.a.	n.a.	n.a.	External	23
injection moulded plastic	Injection moulding	WL-scattering	n.a.	n.a.	n.a.	n.a.	n.a.	Internal	24
plasmonic nanoparticles	Brownian diffusion	WL-diffraction	Binary hash	n.a.	n.a.	n.a.	n.a.	External	25
plasmonic nanoparticles	self-assembly	Laser-Raman	Binary hash	n.a.	n.a.	n.a.	n.a.	External	26
Electrospun nanofiber	electrostatic bending	WL-scattering	perception al hash	256	246	FPR/FNR[j] ~10^{-9}	2.56×10^{7}	Internal	***This work***

[a]CRP, challenge-response pair; [b]k_L, key length; [c]FRR, False Rejection Rate; [d]n.a., not available; [e]WL, white light; [f]FPR, False Positive Rate; [g]SC, Success Rate; [h]BER, Bit Error Rate. [i]FAR, False Acceptance Rate; [j]FNR, False Negative Rate.

S18. Applications of Package Authentication

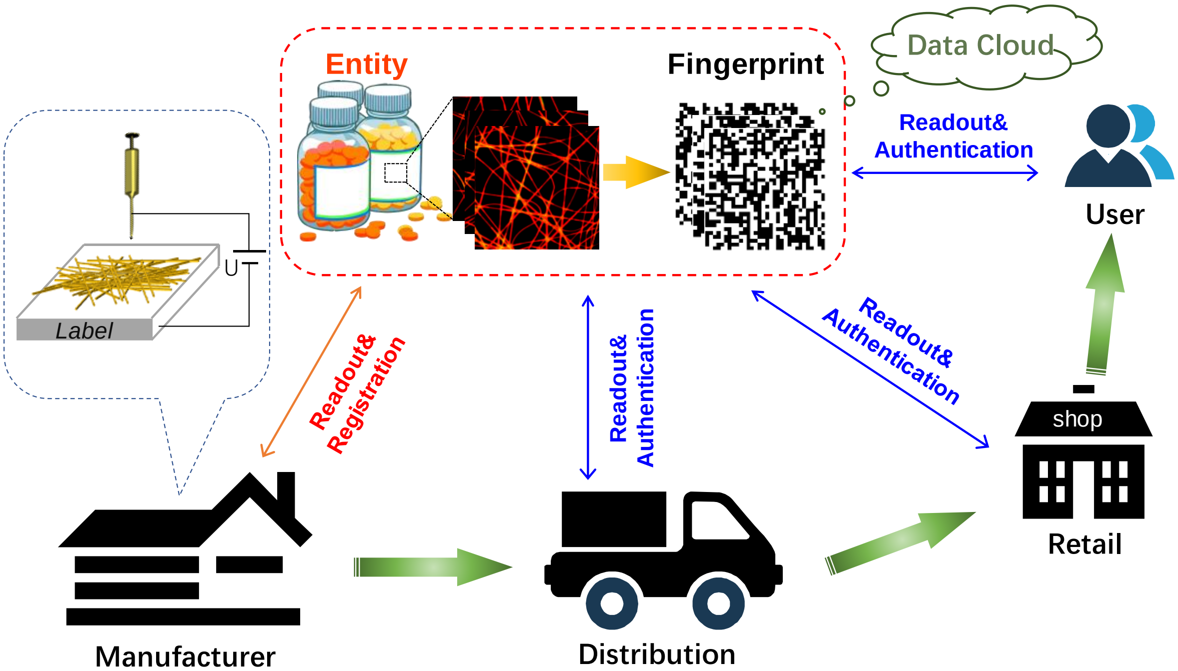

Fig. S14 Each individual label is readout and registered by manufacturer. End users can ensure the provenance and validate the medicine by accessing the enrolled digital keys in a secure database (e.g., cloud server). In addition, this edible PUF could be utilized to provide dose information and manufacturer-determined data, including product information (e.g., dosage strength, dose frequency, and expiration date), manufacturing details (e.g., location, date, batch, and lot number), and distribution.

References:

1 Y. Gao, S. F. Al-Sarawi and D. Abbott, Nat. Electron., 2020, **3**, 81-91.

2 S. Shariati, F. Standaert, L. Jacques and B. Macq, J. Cryptogr. Eng., 2012, **2**, 189-206.

3 R. Arppe and T. J. Sørensen, Nat. Rev. Chem., 2017, **1**, 31.

4 R. Pappu, B. Recht, J. Taylor and N. Gershenfeld, Science, 2002, **297**, 2026-2030.

5 P. Martinez, I. Papagiannouli, D. Descamps, S. Petit, J. Marthelot, A. Lévy, B. Fabre, J. B. Dory, N. Bernier, J. Y. Raty, P. Noé and J. Gaudin, Adv. Mater., 2020, **32**, 2003032.

6 H. Zhang and S. Tzortzakis, Appl. Phys. Lett., 2016, **108**, 211107.

7 Z. Tang, X. Liu, X. Liu, J. Wu, W. Lin, X. Lin and G. Yi, Adv. Eng. Mater., 2022, **24**, 2101701.

8 J. D. Smith, M. A. Reza, N. L. Smith, J. Gu, M. Ibrar, D. J. Crandall and S. E. Skrabalak, ACS Nano, 2021, **15**, 2901-2910.

9 Y. Liu, F. Han, F. Li, Y. Zhao, M. Chen, P. Liu, Y. Li and L. Qian, Nat. Commun., 2019, **10**, 1-9.

10 N. Kayaci, R. Ozdemir, M. Kalay, N. B. Kiremitler, H. Usta, and M. S. Onses, Adv. Funct. Mater., 2021, **32**, 2108675.

11 Y. W. Hu, T. P. Zhang, C. F. Wang, K. K. Liu, Y. Sun, L. Li, C. F. Lv, Y. C. Liang, F. H. Jiao, W. B. Zhao, L. Dong and C. X. Shan, Adv. Funct. Mater., 2021, **31**, 2102108.

12 N. Torun, I. Torun, M. Sakir, M. Kalay and M. S. Onses, ACS Appl. Mater. Interfaces, 2021, **13**, 11247-11259.

13 M. Xie, G. Lin, D. Ge, L. Yang, L. Zhang, J. Yin and X. Jiang, ACS Mater. Lett., 2019, **1**, 77-82.

14 Y. Gu, C. He, Y. Zhang, L. Lin, B. D. Thackray and J. Ye, Nat. Commun., 2020, **11**, 516.

15 J. D. R. Buchanan, R. P. Cowburn, A. Jausovec, D. Petit, P. Seem, G. Xiong, D. Atkinson, K. Fenton, D. A. Allwood and M. T. Bryan, Nature. 2005, **436**, 475.

16 P. Bulens, F. X. Standaert and J. J. Quisquater, IET. Inf. Secur., 2010, **4**, 125-136.

17 H. Cheng, Y. Lu, D. Zhu, L. Rosa, F. Han, M. Ma, W. Su, P. S. Francis and Y.Zheng, Nanoscale, 2020, **12**, 9471-9480.

18 A. Sharma, L. Subramanian and E.A. Brewer, In 18th ACM Conference on Computer and Communications Security, 2011, 99-109.

19 W. Clarkson, T. Weyrich, A. Finkelstein, N. Heninger, J. A. Halderman and E. W. Felten,

In 30th IEEE Symposium on Security and Privacy, 2009, 301-314.

20 J. Xue, T. Wu, Y. Dai and Y. Xia, Chem. Rev., 2019, **119**, 5298-5415.

21 N. Bhardwaj and S. C. Kundu, Biotechnol. Adv., 2010, **28**, 325-347.

22 D. H. Reneker, A. Yarin, E. Zussman, S. Koombhongse and W. Kataphinan, In Chapter 2: Nanofiber manufacturing: toward better process control, ACS Symposium Series, American Chemical Society: Washington, DC, 2006.

23 Y. Feng, Y. Gu, M. Wang, X. Xu, Y. Liu and D. Li, Adv. Mater. Interfaces, 2021, **8**, 2002246.

24 D. Taşcıoğlu, A. Atçı, S. S. Ünlütürk and S. Özçelik, Nanotechnology, 2021, **33**, 95302.

25 A. Esidir, N. B. Kiremitler, M. Kalay, A. Basturk and M. S. Onses, ACS Appl. Polym. Mater., 2022, **4**, 5952-5964.

26 M. S. Kim, G. J. Lee, J. W. Leem, S. Choi, Y. L. Kim and Y. M. Song, Nat. Commun., 2022, **13**, 247.

27 S. Hou, D. Deng, Z. Wang, J. Shi, S. Li and Y. Guo, CCF Trans. HPC, 2021, **3**, 31-56.

28 Y. Cheng, S. Qiang, J. Li, W. Wei, Y. Kuang, W. Zhang, X. Fang, T. Ding, L. Guo, Y. Chen and X. Chen, ACS Appl. Nano Mater., 2022, **5**, 14902-14911.

29 F. He, H. Li, H. Xu, J. Bai, Y. Cheng, X. Meng, W. Zhang, X. Fang, Y. Xu and T. Ding, Phys. Chem. Chem. Phys., 2021, **23**, 388-398.

30 W. Zhu, X. Meng, H. Li, F. He, L. Wang, H. Xu, Y. Huang, W. Zhang, X. Fang and T. Ding, Opt. Mater., 2019, **88**, 412-416.

31 X. Meng, Y. Wang, X. Liu, M. Wang, Y. Zhan, Y. Liu, W. Zhu, W. Zhang, L. Shi and X. Fang, Opt. Mater., 2018, **77**, 48-54.

32 X. Liu, H. Li, L. Shi, X. Meng, Y. Wang, X. Chen, H. Xu,; W. Zhang, X. Fang and T. Ding, J. Mater. Chem. C, 2017, **5**, 10302-10312.

33 J. Bai, Y. Tian, Y. Wang, J. Fu, Y. Cheng, S. Qiang, D. Yu, W. Zhang, K. Yuan and X. Chai, J. Phys. D., 2022, **55**, 205106.

34 P. Samanta and S. Jain, Procedia. Comput., 2021, **185**, 203-212.

35 J. Hou, B. Xu, H. Gao, R. Wang, Text. Res. J., 2018, **88**, 2120-2131.

36 P. Moll, S. Wang, S. Coutandin, J. Fleischer, Text. Res. J., 2021, **91**, 664-680.

37 L. Zhang and W. Yu, Text. Res. J., 2017, **87**, 2263-2274.

38 L. Bassham, A. Rukhin, J. Soto, J. Nechvatal, M. Smid, S. Leigh, M. Levenson, M. Vangel,

N. Heckert and D. Banks, Special Publication (NIST SP), National Institute of Standards and Technology, Gaithersburg, MD, [online], 2010, https://tsapps.nist.gov/publication/get_pdf.cfm?pub_id=906762.

39 J. W. Leem, M. S. Kim, S. H. Choi, S. Kim, S. Kim, Y. M. Song, R. J. Young, Y. L. Kim, Nat. Commun., 2020, **11**, 328.